SOVIET PHYSICS

JETP

A translation of Zhurnal Éksperimental'noĭ i Teoreticheskoĭ Fiziki.

Vol. 11, No. 5, pp. 981-1193 (Russ. orig. Vol. 38, No. 5, pp. 1361-1656, May, 1969) Nov.,1960

ENERGY SPECTRA OF THE ELECTRON-PHOTON COMPONENT IN EXTENSIVE ATMOSPHERIC SHOWERS NEAR THE SHOWER AXIS

O. I. DOVZHENKO, S. I. NIKOL'SKIĬ, and I. V. RAKOBOL'SKAYA

P. N. Lebedev Physics Institute, Academy of Sciences, U.S.S.R.

Submitted to JETP editor December 18, 1959

J. Exptl. Theoret. Phys. (U.S.S.R.) **38**, 1361-1369 (May, 1960)

A cloud chamber with lead plates was employed to investigate the electron-photon component of extensive atmospheric showers at sea level. Showers containing on the average 8×10^3, 1.2×10^4, and 3×10^4 particles and passing at distances of $0 - 3$ m from the chamber were selected. Energy spectra of the electron-photon component were derived, and the fraction of high-energy electrons and photons at distances of $0 - 3$ m and $0 - 0.3$ m from the shower axis were determined. The lateral distribution of high-energy electrons and photons at distances of $0 - 0.3$ m from the axis was also obtained.

A study of the energy spectra and of the lateral distribution of the electron-photon component of extensive atmospheric showers (EAS) has previously been carried out both at sea level[1] and at high altitudes.[2,3] In these studies the region between 0 and 10 m from the shower axis was investigated. Comparison of the obtained spectra with those calculated according to the cascade theory, assuming the energy of the generating particle to be infinite,[3] showed that the experimental spectra near the shower axis are poor in high-energy electrons,* particularly at very small distances from the shower axis (mainly $0 - 1$ m), i.e., in the actual shower core.

However, previous studies[1,2] did not permit a sufficiently accurate separation of shower cores, and few cases in which the EAS passed at a distance up to 1 m from the cloud chamber were registered. Therefore, the energy spectra of the electrons and photons in this region were investigated with insufficient accuracy.

In reference 3 showers with a number of particles $\bar{N} = 2 \times 10^5$ were investigated. For small distances between the shower axis and the cloud chamber a very large particle flux density (~ 100 per 0.15 m^2) was observed in the upper section. Therefore, a separation of discrete particles was difficult, a fact which lowered the precision of the obtained results. The results of references 1 and 3 differ markedly from each other. It became, therefore, essential to investigate in detail the electron and photon energy spectra in EAS at sea level in the region $0 - 3$ m from the shower axis, choosing showers with a small particle flux density.

MEASUREMENT METHOD

A rectangular cloud chamber[4] containing lead plates successively 1, 2, 2.5, 2, 2.5, and 1.5 cm thick (a total thickness of 120 g/cm^2) was used as the registering device.

The energy of the electrons and photons was determined from the total number of particles in the cascade showers which they produced in the lead

*It must here be noted that the theoretical integral spectra were calculated for electrons only. However, an experimental separation of electrons and photons in the cloud chamber has until now proved impossible because of the large conversion probability in the upper wall of the chamber.

plates of the chamber (cf. references 1 and 3). In practice account was taken not of the total number of particles moving forward in all sections within an angle of 180°, but only of particles in the region of the shower maximum. At the shower boundary where one or two particles should have been observed, the latter were strongly scattered in the lead and it was impossible to count them reliably. Owing to the error in counting the number of scattered particles, the electron energy may be about 10% too low.

The monitoring device was chosen with a view to making a more efficient separation of EAS with axes close to the cloud chamber possible. Two alternate methods for the selection of showers were employed. (The general plan of the array is shown in Fig. 1.)

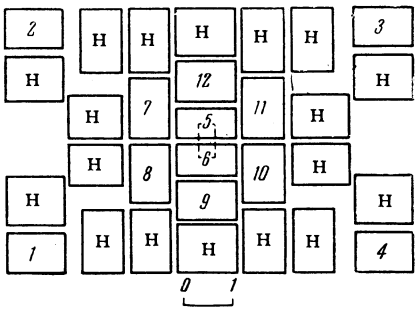

FIG. 1. General plan of the array. The cloud chamber is represented by the dashed rectangle at the center. The counters of the monitoring system are in trays 1–6; H – hodoscopes for the first monitoring system; 7 – 12 are the trays for the second monitoring system.

1. In the first method the EAS was separated from the general flux of cosmic particles with the aid of counters connected to coincidence and anticoincidence circuits. The group of counters 5 — 6 (at the center of the array) was connected to four channels of a coincidence circuit. The area of the counters connected to one channel amounted to 0.16 m^2. Each group of counters 1 — 4 (located at a distance of 3 m from the center) was connected to three channels of a triple coincidence circuit; the counter area for each channel was 0.13 m^2. A shower was recorded only in the event that a fourfold coincidence in the counters of the group 5 — 6 was not accompanied by a threefold coincidence in any one of groups 1 — 4. To determine the location of the EAS axis and the number of particles in the shower a GK-7 hodoscopic device consisting of 24 groups of 12 hodoscope counters each (counter area σ_C = 330 cm^2) was employed. The hodoscopic device made it possible to pick out showers whose axes passed not further than 3 m from the chamber; the precision in locating the axis was ~ 1 m.

An earlier[5] theoretical calculation distribution of the distances of the EAS axes from the center of the array for a given monitoring system indicated that 50% of all the showers registered by the array should have axes located 0 — 3 m from the chamber. In the experiment, however, 30% of all shower axes were found within a radius of 3 m. Such a discrepancy between the experimental and calculated values can be explained if account is taken of the fact that the number of hodoscopes fired upon passage of showers with $\leq 3 \times 10^3$ particles was insufficient for a determination of the shower-axis location. In the processing of the hodoscopic data this caused such events to be counted among the showers with axes more than 3 m from the chamber.

In Fig. 2 the solid line indicates the distribution of the distances from the cloud chamber to the axes of the showers chosen for processing. Showers with $\bar{N} \sim 8 \times 10^3$ were registered most efficiently.

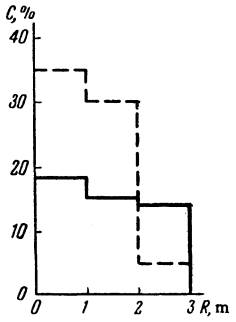

FIG. 2. The distribution of the numbers C of EAS by the distances R of their axes from the cloud chamber. The solid line indicates the experimental distribution for the first monitoring system; the dashed line indicates the distribution for the second monitoring system, obtained by theoretical calculations.

2. In the second method of measurement an extensive atmospheric shower was recorded only when the particle flux density above the cloud chamber (registered by the counters) exceeded the particle flux density registered by counter groups located away from the center.

Groups 1 — 4 contained 12 counters each, while groups 5 and 6 had 18 each (cf. Fig. 1). The area of each counter was 100 cm^2 in the first measurement series and 38 cm^2 in the second. In the event of an EAS passing through the array, a voltage pulse, of amplitude proportional to the number of counters fired in a given group, was formed in each of the electronic circuits connected to the counter groups 1 — 6. If we denote the number of counters fired in the i-th group by m_i, then the condition for the registration of a shower can be expressed as

$$\sum_{i=5}^{6} m_i - \sum_{j=1}^{4} m_j \geqslant 6; \qquad m_5 \geqslant 2, \qquad m_6 \geqslant 2.$$

To determine the total number of particles in the recorded showers, a hodoscopic device, consisting of six groups of 24 counters each (the

area of each counter was 100 cm^2) was employed. The distribution of the shower-axis distances from the cloud chamber (indicated in Fig. 2 by the dashed line) was calculated for the given monitoring system.[5]

In the first series of measurements the monitoring system registered most efficiently showers with $\bar{N} = 1.2 \times 10^4$, in the second series — showers with $\bar{N} = 3 \times 10^4$ particles.* The axes of 70% of all recorded showers were not farther than 3 m from the chamber.

To check the effect of the passage through the roof over the building in which the measurements were carried out, one tray of counters, connected to the hodoscopic device, was placed on the roof.

MEASUREMENT RESULTS

In all, 2370 EAS were registered with the first monitoring system, while 1830 showers with $\bar{N} = 1.2 \times 10^4$ particles (after 680 hours of operation) and 436 showers with $\bar{N} = 3 \times 10^4$ (after 420 hours of operation) were registered with the second monitoring system. The mean flux density of charged particles, determined with the aid of the hodoscopes on the roof, was 20% less than the density in the room.

The data from the hodoscopes of the first monitoring system yielded the lateral distribution of charged particles in the showers with $\bar{N} = 9 \times 10^3$, as shown in Fig. 3. It can be seen that this distribution has the form

$$\rho(>0) \sim r^{-n}, \qquad n = 1.0 \pm 0.1.$$

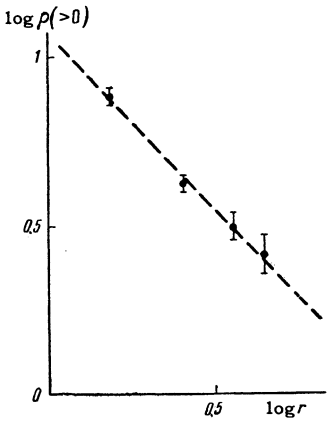

FIG. 3. Lateral distribution of charged particles in showers with $\bar{N} = 9 \times 10^3$; r is the distance from the shower axis in meters, $\rho(>0)$ is the electron flux density per m^2.

The measurements yielded the integral energy spectra of the electron-photon component, as shown in Fig. 4. The flux density per square meter of

*This was achieved by decreasing the counter area (by a factor of 2.6) in the monitoring system (we assumed the exponent κ in the shower number-of-particles spectrum to be constant).

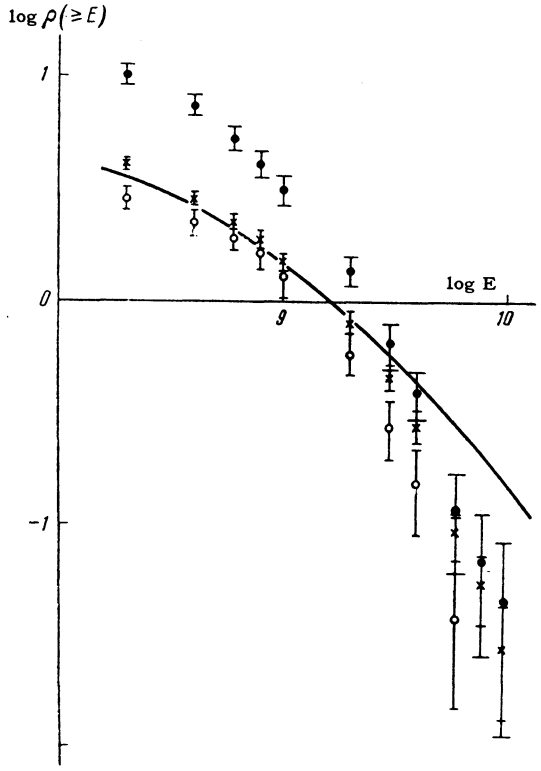

FIG. 4. Integral energy spectra of electrons and photons. $\rho(\geq E)$ is the flux density of electrons and photons with energies $\geq E$ (per m^2) in one shower (the energy E is expressed in ev). The solid curve is the theoretical curve for s = 1.2 and $E_0 = 10^{15}$ ev, normalized in terms of the experimental results for $E = 10^9$ ev and $\bar{N} = 1.2 \times 10^4$; ●–$\bar{N} = 3 \times 10^4$, ×–$\bar{N} = 1.2 \times 10^4$, and ○–$\bar{N} = 8 \times 10^3$.

electrons and photons with energies higher than E was determined as follows:

$$\rho(\geq E) = N(\geq E)/C, \qquad N(\geq E) = \int_E^\infty (N(E)/\sigma(E))\,dE,$$

where C is the number of showers, $\sigma(E)$ — the effective area of the chamber for electrons with energy E, and N(E) the number of such electrons and photons.

The electron and photon energy spectrum thus obtained can be represented in the form

$$\rho(\geq E) = \text{const}/E^\gamma \quad \begin{matrix} \gamma = 0.65 \pm 0.05 \text{ for } E = 2 \cdot 10^8 - 10^9 \text{ ev}, \\ \gamma = 1.8 \pm \qquad \text{for } E = 2 \cdot 0^9 - 10^{10} \text{ ev}. \end{matrix}$$

This agrees with our earlier results,[3] and also with the results of the Japanese authors[6] who, for somewhat larger distances (1 — 5 m), obtained $\gamma = 1$ for energies of $2 \times 10^8 - 10^9$ ev, and $\gamma = 1.5$ to 2 for energies of $10^9 - 5 \times 10^9$ ev.

To check whether the energy spectrum of the particles in a shower varies with the number of particles $\bar{N}$ in the shower, we plotted the ratio of the electron and photon flux density for showers with $\bar{N} = 3.0 \times 10^4$ and $\bar{N} = 1.2 \times 10^4$ (cf. Fig. 5).

TABLE I

	Present work			[2]	[3]	[4]
$\bar{N}$	$8\cdot10^3$	$1.2\cdot10^4$	$3\cdot10^4$	10^5—$3\cdot10^6$	$6.4\cdot10^4$	$8\cdot10^4$—$3\cdot10^6$
$\rho(\geqslant 10^9)$, m^{-2}	1.32	1.90	4.08			
$\rho(>0)$, m^{-2}	8	13	30			
Δ, %	16±4	15±3	13±3	11±5	10±1	12±1

TABLE II

r, m	0—1	1—2	2—3	3—6	6—10	10—20
ρ, m^{-2}	3.66	1.01	0.48	0.185	0.027	0.008
ρC	132	30.3	2.15	0.65	0.1	0.05
$10^{-4}\rho C\bar{N}$	264	73	8.6	6.5	3.0	2.5

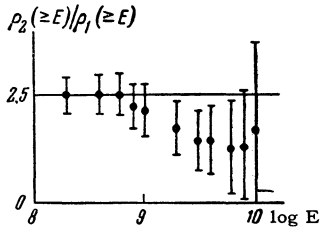

FIG. 5. The ratios of the flux densities of electrons and photons with energies $\geqslant E$ for showers with $\bar{N} = 3 \times 10^4$ (ρ_2) and $\bar{N} = 1.2 \times 10^4$($\rho_1$). The energy is given in ev.

It can be seen that the fraction of high-energy ($E \geq 2 \times 10^9$ ev) electrons and photons is smaller in showers with $\bar{N} = 3 \times 10^4$ than in showers with $\bar{N} = 1.2 \times 10^4$.

In addition, the fraction of high-energy electrons and photons relative to all the electrons in the shower was determined for showers with various numbers of particles. As before, this fraction was found from the ratio of the flux density of electrons and photons with $E \geq 10^9$ ev, obtained from the cloud chamber data to the flux density of all electrons, obtained from the data of the hodoscopic counters:*

$$\Delta = \rho(\geqslant 10^9)/\rho(>0).$$

The value of Δ obtained is listed in Table I together with data by others, pertaining to a distance 0 — 3 m from the shower axis. As can be seen from Table I, all the results obtained for showers with different numbers of particles agree with each other within the limits of the experimental errors.

In working with the second monitoring system, we could not determine the location of the shower axis. To estimate the number of high-energy electrons in the region of 0 — 3 m from the chamber, the theoretical lateral distribution of electrons with $E \geq 10^9$ ev, obtained from cascade theory for a value of $s = 1.5$, was employed.

This distribution is listed in Table II (second line). The third line was obtained after taking into account the experimentally observed distribution of the distances of the recorded shower from the cloud chamber. The fourth line includes an allowance for the change in the mean number of particles $\bar{N}$ in a shower with increasing distance from the axis to the chamber. From Table II it can be seen that for this monitoring system no more than 4% of the total of recorded electrons with $E \geq 10^9$ ev will be registered at a distance of more than 3 m from the axis. Using this estimate, we obtained the data listed in Table I for the region of 0 — 3 m.

It has been assumed previously[7] that near the EAS axis the fluctuations of the high-energy electron and photon flux density, registered by a cloud chamber, do not have a Poisson distribution, and this partially explains the discrepancy between the results of references 1 and 3. In the present investigation we checked the validity of that assumption. For this purpose the 1800 EAS recorded with the second monitoring system were divided, in the order in which they had been registered, into 36 groups of 50 showers each. The number of electrons and photons with $E \geq 10^9$ ev in each group was calculated, and the distribution of the obtained values, shown in Fig. 6, was then found. The smooth curve in the figure represents Poisson's integral distribution, corresponding to the known mean number of particles per effective chamber area. It is clear that the experiment does not yield a Poisson distribution.

Later we excluded from consideration those

*The flux density $\rho(>0)$ was determined from the cloud-chamber measurements. On the average $\rho(>0)$ obtained from the chamber measurements is 20% higher than that obtained from the hodoscopic data. This is explained by the effect of the passage through the upper wall of the chamber. The effect of the passage through the roof of the building is still not accounted for in these calculations; the correction for this effect is introduced in the comparison with the theory.

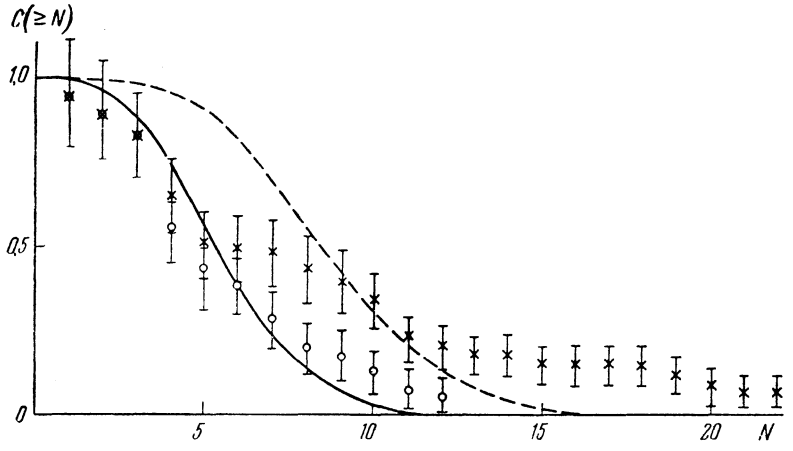

FIG. 6. Integral distribution of 50 EAS by the number N of electrons and photons with energies $\geqslant 10^9$ ev recorded in the cloud chamber; x – experimental points for all showers, o – points obtained on excluding the 12 cases in which the shower core passed through the chamber. The curves are the Poisson distributions for the corresponding cases.

12 cases* in which the EAS cores passed through the chamber, and the distribution, also shown on Fig. 6, was plotted. This turned out to be close to a Poisson distribution. Thus, as was assumed, the main deviation from a Poisson distribution is connected with the fact that in the relatively few cases when an EAS core passes through the cloud chamber, the flux density of the high-energy electrons and photons exceeds the mean flux density of these particles within the investigated distance of 0 – 3 m.

The passage of a core through the cloud chamber was identified by simultaneous satisfaction of three criteria:

1. The electron and photon flux density, determined from the measurements in the chamber, had to exceed at least by one order of magnitude the electron flux densities determined with the aid of the hodoscopes located near the chamber.

2. The number of high-energy ($\geq 10^9$ ev) electrons and photons observed in the chamber had to be greater than 7.

3. Electrons and photons with an energy $\geq 6 \times 10^9$ ev had to be observed in the chamber.

The mean flux density ρ ($\geq 10^9$) of high-energy electrons and photons was 70 m^{-2} in the shower core and 1.25 m^{-2} 0.3 – 3 m from the axis. Therefore, the fraction of high-energy particles (Δ) in the total electron and photon flux depends strongly on whether the events of the passages of cores through the chamber ($\Delta = 15\%$) are included in the general statistics or whether they are not included (in which case $\Delta \approx 10\%$). From this it is clear that the apparent "softening" of the experimental spectrum for showers with $\bar{N} = 3 \times 10^4$ particles compared to showers with $\bar{N} = 1.2 \times 10^4$ can be explained by the fact that in the second series of experiments not even one passage of a shower core through the chamber was registered (the passage of two or three cores was expected from the calculations).

In view of the fact that the number of high-energy electrons and photons $N(\geq E)$ which entered the cloud chamber did not have a Poisson distribution, we did not take the error in the calculation of $N(\geq E)$ to be of the form $\sqrt{N}$, but applied the formulas of the general theory of errors. We considered the number of high-energy electrons $N(\geq E)$ obtained by us to be a linear combination of the form

$$N = \rho_1 n_1 + \rho_2 n_2 + \ldots + \rho_n n_n,$$

where n_i is the number of events when ρ_i electrons with an energy $\geq E$ are observed in the chamber. The mean-square error of the arithmetic mean of the electron flux density is then equal to

$$\sigma = \left[\frac{1}{n(n-1)} \sum_{i=1}^{n} \varepsilon_i^2\right]^{1/2},$$

where ϵ_i is the deviation of the observed value of ρ from the arithmetic mean: $\epsilon_i = \rho_i - \bar{\rho}$. The value σ thus calculated is almost twice as large as the value of $\sqrt{N}/C$.

We plotted the electron and photon energy spectrum in the region of the EAS axis at distances of 0 – 0.3 m from the axis for the 12 cases of the passage of the core through the chamber (cf. Fig. 7). For such small distances the spectrum exponent γ is 0.34 ± 0.05 in the 2×10^8- to 10^9-ev energy range, and 1.3 ± 0.2 in the 2×10^9- to 10^{10}-ev energy range. The fraction of particles with energies $\geq 10^9$ ev for these cases is $\Delta = (56 \pm 14)\%$. The average energy per charged particle is $\bar{E} \sim 3 \times 10^9$ ev in the region of the shower axis and $\bar{E} \sim 4 \times 10^8$ ev at distances of 0.3 – 3 m from the axis.

Using the results of our measurements, we found the lateral distribution of high-energy elec-

*This number corresponds to that calculated for the given monitoring system.

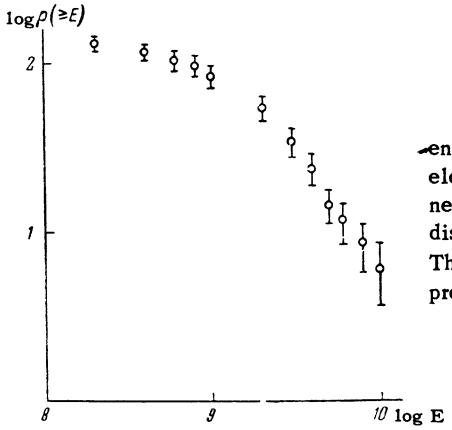

FIG. 7. Integral energy spectrum of the electrons and photons near the EAS axis at distances of 0 – 0.3 m. The energy is expressed in ev.

trons and photons at distances of 0 — 0.3 m from the shower axis. As the shower axis we took the region with the highest energy flux density, which also coincided for the most part with the largest particle density. For electrons and photons with an energy $\geq 10^9$ ev (cf. Fig. 8)

$$\rho(\geqslant 10^9) \sim r^{-n}, \qquad n = 1.2 \pm 0.3.$$

In reference 3 a value n = 1.6 ± 0.3 was obtained for particles of the same energy at distances of 1 — 7 m from the shower axis. In the work of the Japanese authors[6] the lateral distribution of electrons and photons with $E \geq 10^9$ ev at distances of 1 — 7 m from the axis was found to be

$$\rho(\geqslant 10^9) \sim r^{-1.5}.$$

As can be seen, the data obtained in the present paper are in agreement with previous results.

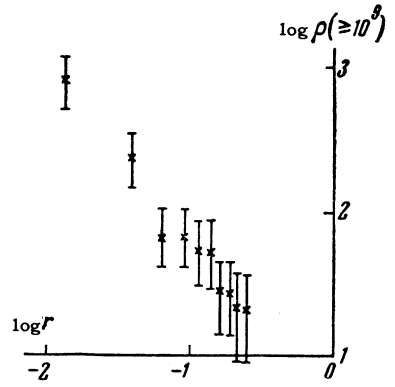

FIG. 8. The lateral distribution of high-energy electrons and photons at distances $r \leqslant 0.3$ m from the shower axis. $\rho(\geqslant 10^9)$ is the flux density of electrons and photons with $E \geqslant 10^9$ ev per m^2.

To compare the results obtained with cascade theory, calculations of the energy spectra of the electrons in the shower were carried out. It was assumed that the electron-photon component is in equilibrium with the nuclear-active component, and that the nuclear-active component produces protons with $E = 10^{11}$ ev (or 10^{12} ev) with a probability which decreases as $\exp(-\mu t)$. To carry out such calculations we used the results of reference 8. A depth of 30 radiation units was taken as the observation level, and it was assumed that $\bar{s} = 1.2$. The spectra obtained both for $E = 10^{12}$ ev and for $E = 10^{11}$ ev coincide with those calculated by us previously (for s = 1.2) for a generating particle of infinite energy and, as previously, differ considerably from the experimental results.

Thus, on the basis of all that has been said, the following conclusions can be drawn: 1) no change was observed in the fraction of high-energy electrons and photons with increasing total number of particles in the recorded atmospheric showers; 2) the experimentally observed fraction of high-energy electrons and photons is much smaller than its calculated value, obtained for an infinite initial energy and under the assumption of equilibrium between the electron-photon and the nuclear-active component of the shower. The latter conclusion is apparently explained by the fact that the initial conditions of the formation and development of the electron-photon component in an EAS are poorly accounted for in the theoretical calculations.

In conclusion, the authors express their deep gratitude to G. T. Zatsepin, I. P. Ivanenko, and L. I. Sarycheva for a discussion of the obtained results, and also to D. F. Rakitin, O. N. Novoselov, I. A. Ivanovskaya, B. M. Mozhaev, and L. K. Bocharov who took part in the measurements at various stages of the work.

[1] Ivanovskaya, Kulikov, Rakobol'skaya, and Sarycheva, JETP **33**, 358 (1957), Soviet Phys. JETP **6**, 276 (1958).

[2] Hazen, Williams, and Randall, Phys. Rev. **93**, 578 (1954).

[3] Danilova, Dovzhenko, Nikol'skiĭ, and Rakobol'skaya, JETP **34**, 541 (1958), Soviet Phys. JETP **7**, 374 (1958).

[4] I. A. Ivanovskaya and A. G. Novikov, J. Tech. Phys. **26**, 209 (1956), Soviet Phys.-Tech. Phys. **1**, 206 (1956).

[5] Dovzhenko, Nikol'skiĭ, and Rakobol'skaya, JETP **36**, 17 (1959), Soviet Phys. JETP **9**, 11 (1959).

[6] Kameda, Toyoda, and Maeda, Cosmic-Ray Research **3**, 470 (1958), in Japanese.

[7] I. A. Ivanovskaya and I. V. Rakobol'skaya, JETP **35**, 1583 (1958), Soviet Phys. JETP **8**, 1108 (1959).

[8] S. Z. Belen'kiĭ and I. P. Ivanenko, Usp. Fiz. Nauk **69**, 591 (1959), Soviet Phys. Uspekhi **2**, 912 (1960).

Translated by Z. Barnea
266

ERRATA TO VOLUME 10

page	reads	should read
Article by A. S. Khaĭkin		
1044, title	. . . resonance in lead	. . . resonance in tin
6th line of article	~ 1000 oe	~ 1 oe
Article by V. L. Lyuboshitz		
1223, Eq. (13), second line	$\ldots-\mathrm{Sp}_{1,2}\mathscr{E}(\mathbf{e}_1)$	$\ldots-\mathrm{Sp}_{1,2}\mathscr{E}(\mathbf{e}_2)\ldots$
1226, Eq. (26), 12th line	$\cdots\{(\mathbf{p}+\mathbf{q},\ \mathbf{p}$	$\cdots\{(\mathbf{p}+\mathbf{q},\mathbf{p})-(\mathbf{p}+\mathbf{q},\mathbf{n})\cdot(\mathbf{pn})\}$
1227, Eqs. (38), (41), (41a) numerators and denominators	$(\mathbf{p}^2-\mathbf{q})$	$(\mathbf{p}^2-\mathbf{q}^2)^2$
1228, top line	$\mathbf{m}_2=\dfrac{\mathbf{q}_1-\mathbf{p}_1}{\mathbf{q}_1-\mathbf{p}_1}$	$\mathbf{m}_2=[\mathbf{m}_3\,\mathbf{m}_1]$

ERRATA TO VOLUME 12

Article by Dzhelepov et al.		
205, figure caption	54	5.4
Article by M. Gavrila		
225, Eq. (2), last line	$-2\gamma\Theta^{-4}\,1/8$	$-2\gamma\Theta^{-4}-1/8$
Article by Dolgov-Savel'ev et al.		
291, caption of Fig. 5, 4th line	$p_0 = 50\times10^{-4}$ mm Hg	$p_0 = 5\times10^{-4}$ mm Hg.
Article by Belov et al.		
396, Eq. (24) second line	$\ldots-(4-2\eta)\sigma_1+\ldots$	$\ldots+(4-2\eta)\sigma_1+\ldots$
396, 17th line (r) from top	. . less than 0.7	. . less than 0.07
Article by Kovrizhnykh and Rukhadze		
615, 1st line after Eq. (1)	$\omega_{0e}^2 = 2\pi e^2 n_e/m_e,$	$\omega_{0e}^2 = 4\pi e^2 n_e/m_e,$
Article by Belyaev et al.		
686, Eq. (1), 4th line	$\ldots b_{\rho_2 m_2}'(s_2')+\cdots$	$\ldots b_{\rho_1 m_1}'(s_1')+\cdots$
Article by Zinov and Korenchenko		
798, Table X, heading of last column	$\sigma_{\pi^-\to\pi^+}=$	$\sigma_{\pi^-\to\pi^-}=$
Article by V. M. Shekhter		
967, 3d line after Eq. (3)	$s\equiv 2m_pE+m_p^2$	$s\equiv(2m_pE+m_p^2)^{1/2}$
967, Eq. (5), line 2	$+(B_V^2+B_A^2)\ldots$	$+(B_V^2+B_A^2)Q\ldots$
968, Eq. (7)	$\ldots(C_V^2+C_A^2).$	$\ldots G_V^2+C_A^2-Q^2(B_V^2+B_A^2).$
968, line after Eq. (7)	for $C_V^2+C_A^2\equiv\ldots$	for $C_V^2+C_A^2-Q^2(B_V^2+B_A^2)\equiv\ldots$
Article by Dovzhenko et al.		
983, 11th line (r)	$\gamma = 1.8\pm$	$\gamma = 1.8\pm0.2$
Article by Zinov et al.		
1021, Table XI, col. 4	−1,22	1,22
Article by V. I. Ritus		
1079, line 27 (1)	$-\Lambda_{\pm}(t),$	$\Lambda_{\pm}(t),$
1079, first line after Eq. (33)	$\frac{1}{2}(1+\beta).$	$\frac{1}{2}(1\pm\beta).$
1079, 3d line (1) from bottom	$\ldots\Re(q'p;\ pq')\ldots$	$\ldots\Re(p'q;\ pq')\ldots$
Article by R. V. Polovin		
1119, Eq. (8.2), fourth line	$U_{0x}u_x g(\gamma)-[\gamma\cdots$	$-U_{0x}u_x g(\gamma)\,[\gamma\ldots.$
1119, Eq. (8.3)	$\cdots\text{sign } u,$	$\cdots\text{sign } u_g.$
Article by V. P. Silin		
1138, Eq. (18)	$\cdots+\frac{4}{5}c^2k^2$	$\cdots+\frac{6}{5}c^2k^2.$